



Preparation, characterization, and application of Ti/TiO₂-NTs/Sb-SnO₂ electrode in photo-electrochemical treatment of industrial effluents under mild conditions

Anantha N Subba Rao¹ · Venkatesha T Venkatarangaiah²

Received: 31 October 2017 / Accepted: 27 December 2017 / Published online: 9 February 2018
© Springer-Verlag GmbH Germany, part of Springer Nature 2018

Abstract

Ti/TiO₂-NTs/Sb-SnO₂ electrode was prepared by gradient pulsed electrodeposition, and its electrochemical properties were evaluated. The catalytic activity and reusability of the electrode were tested by electrochemical oxidation (EO) and photoelectrochemical oxidation (PEO) of organics present in textile industry wastewater (TWW) and coffee bean processing industry wastewater (CWW). COD removal of ~41% was achieved after 5-h electrolysis under a constant applied current density of 30 mA cm⁻² for TWW and 50 mA cm⁻² for CWW. Nearly 14 and 18% increment in COD removal was observed under PEO for TWW and CWW, respectively. The turbidity of TWW reduced from 15 to ~3 NTU and the turbidity of CWW reduced from 27 to ~3 NTU by both EO and PEO. The % COD removal observed after 5-h electrolysis remained consistent for 7 repeated cycles; however, the catalytic activity of the electrode reduced gradually. These results suggested that the Ti/TiO₂-NTs/Sb-SnO₂ can be a potential electrode for the treatment of industrial wastewater.

Keywords TiO₂ nanotube · Textile industrial wastewater · Mixed metal oxide · Electrochemical oxidation · Degradation

Introduction

Chemical and biological/microbial methods are the most prevalent wastewater treatment methods used in the industries and municipal wastewater treatment plants. The refractory organic pollutants are reluctant to degradation by biological methods, whereas physicochemical and chemical treatments necessitate the addition of chemical reagents for the removal of organic pollutants (Anantha and Venkatesha 2014; Martinez-Huitle et al. 2015; Radjenovic and Sedlak 2015). On the contrary, the electrochemical oxidation (EO)—an advanced oxidation process—is a promising technology for the abatement of

persistent organic compounds without the addition of any chemical reagent (Martinez-Huitle and Ferro 2006; Panizza and Cerisola 2009). Strong oxidants, especially hydroxyl radical (•OH), are generated in situ on the immobilized electrode surface by water electrolysis (Martinez-Huitle and Ferro 2006). The •OH (E° = 2.8 V vs SHE) is capable of oxidizing almost any organic molecule into CO₂ and H₂O. However, the oxygen evolution reaction (OER) closely competes with the •OH generation during electrolysis (Weiyi et al. 2014; Jungeng et al. 2016). Thus, the selection of a suitable electrode with high oxygen evolution potential (OEP), stability, and excellent electrocatalytic activity for •OH generation is crucial in enhancing the efficiency EO (Weiyi et al. 2014).

The Ti-based mixed metal oxide anodes have evolved markedly since the advent of dimensionally stable anodes (DSAs) (Anantha and Venkatesha 2014; Weiyi et al. 2014). DSA type electrodes like Ti/IrO₂, Ti/RuO₂, Ti/Ru_{0.3}Ti_{0.7}O₂, Ti/Sb-SnO₂-Ir, Ti/RuO₂-SnO₂, Ti/IrO₂-SnO₂ are now commercially available (Weiyi et al. 2014). Several research groups have tested the proficiency of EO in the treatment of wastewater from tannery (Basha et al. 2009; Carla et al. 2010), pharmaceutical, coking (Wang et al. 2008), paper and textile industries (Patricia et al. 2004), phenol-formaldehyde resin

Responsible editor: Bingcai Pan

✉ Venkatesha T Venkatarangaiah
drtvvenkatesha@yahoo.co.uk

¹ Department of Chemistry, Ballari Institute of Technology and Management, Jnana Gangotri Campus, Ballari-Hosapete Road, Near Allipura, Ballari, Karnataka 583104, India

² Department of P.G. Studies and Research in Chemistry, School of Chemical Sciences, Kuvempu University, Shankaraghatta, Shimoga, Karnataka -577451, India

and bulk drug manufacturing industries (Rajkumar and Palanivelu 2004), industrial cartons (Errami et al. 2013), carwash outflow (Humberto et al. 2015), latrine wastewater (Justin et al. 2016), olive mill wastewater (Chatzisyseon et al. 2009) using DSA-type anodes or boron-doped diamond anode. The major disadvantages associated with these anodes are low OEP and high cost. Furthermore, high concentration of NaCl was used in these studies to increase the conductivity and facilitate the indirect electrochemical oxidation by the in situ generation of active chlorine species (Cl_2 , OCl^- , HOCl , ClO_3^-).

In this regard, an inexpensive electrode with superior electrocatalytic activity and high oxygen evolution potential is of huge demand. Despite Ti/SnO₂ electrode qualifies the prerequisite properties of an anode, its practical application is constrained by short service life. In order to improve its stability, different research teams modified SnO₂ by (i) doping with metals and non-metals, (ii) using combinations of different fabrication techniques, and (iii) incorporation of an inter-layer between the active SnO₂ layer and the substrate (Martinez-Huitle and Ferro 2006; Guohua et al. 2009; Peiqiang et al. 2009; Xiao et al. 2009; Fengping et al. 2011; Hao et al. 2012; Martinez-Huitle et al. 2015; Weiyi et al. 2015). It is reported that the stability of SnO₂ anode can be enhanced substantially by loading SnO₂ into the highly ordered TiO₂-nanotube (TiO₂-NTs) array generated on Ti substrate. The nano-tubular template coated with SnO₂ forms a stable stacked structure that binds the active metal oxide layer to the Ti substrate (Peiqiang et al. 2009; Yong et al. 2010; Anlin et al. 2017; Anantha et al. 2017). Furthermore, SnO₂ is a semiconductor photocatalyst which absorbs UV light in the range of 326–355 nm (Fan et al. 2009). The electron-hole pair generated on UV irradiation can be effectively separated by the application of positive bias to the metal oxide electrode. The photo-generated holes are capable of oxidizing H₂O into $\cdot\text{OH}$. Additionally, the oxygen evolved at the anode surface also participates in the photochemical reaction in presence of UV radiation (Fan et al. 2009). The combined photo-electrochemical method for wastewater treatment is thus expected to be highly efficient. The objective of the present study is to fabricate a stable TiO₂-NTs/Sb-SnO₂ electrode by gradient pulsed electrodeposition technique and to evaluate the treatability of textile industrial wastewater (TWW) and coffee bean processing unit wastewater (CWW) by EO and PEO under mild operating conditions.

Methods and materials

Effluents

The TWW was collected from a local textile industry M/s Shahi exports pvt. Ltd. Bangalore, India. The as-received effluent was highly turbid and blue in color. It was mainly

composed of fabric residues, surfactant/softeners, dyes, and salts. The exact components of the effluent and the dyes used were not revealed. The wastewater from coffee bean processing unit (CWW) was obtained from a coffee plantation site at Chikkamagaluru, India. The effluent from this site possessed strong odor and mainly consisted of coffee plant leaf residues, coffee bean and leaf extract, pesticides, soil leachate. The initial characteristics of the effluents are given in Table 1.

Preparation of TiO₂-NTs/Sb-SnO₂ electrode

TiO₂-NTs was prepared using the procedure described elsewhere with some modifications (Nishanthi et al. 2015). Titanium metal foil of thickness 0.25 mm and dimension 20 mm × 15 mm was subjected to ultrasonication successively in acetone, ethanol, and ultrapure water for 10 min in each solvent and then etched in a solution containing 4:1:5 ≡ HNO₃ (69–72%): HF (40%): H₂O for 15 min. TiO₂-NTs array was prepared by anodization of Ti foil in 100 mL of ethanediol-water (98:2) mixture containing 0.5 g NH₄F. The anodization was carried out at a working potential of 30 V between Ti and Pt foil for 60 min in a Teflon beaker under vigorous stirring. The Ti foil was used as anode and Pt foil as cathode. The dimension of the electrode was 10 mm × 10 mm and the electrodes were separated by 15 mm. After anodization, the Ti foil was thoroughly washed with ultrapure water. To remove the debris possibly accumulated on the surface of amorphous TiO₂-NTs film, it was subjected to ultrasonication for 30 s and then annealed at 500 °C for 60 min under heating and cooling rate of 5 °C min⁻¹.

The TiO₂-NTs/Sb-SnO₂ was prepared by electrodeposition in 100 mL of aqueous electrolyte containing SnCl₂·2H₂O (2.2 g), SbCl₃ (0.22 g), and citric acid (2.2 g). In order to lower the surface tension, 0.05 wt% of (3-aminopropyl) trimethoxysilane was added to the electrolyte. TiO₂-NTs substrate was polarized for 3 min at -1.5 V vs SCE in an aqueous electrolyte containing 0.5 M Na₂SO₄ to improve its conductivity (Zhen et al. 2015). Then, it was rinsed with water, and an area of 10 mm × 10 mm was vertically immersed in the

Table 1 Characteristics of the effluents

Effluent	Textile	Coffee
pH	7.51	4.83
Conductivity (mS cm ⁻¹)	2.19	1.45
COD (mg L ⁻¹) before filtration	1834 ± 40	3362 ± 56
COD ^a (mg L ⁻¹) after filtration	237 ± 14	686 ± 27
TSS (mg L ⁻¹)	1000 ± 48	2250 ± 140
TDS (mg L ⁻¹)	1564 ± 60	2940 ± 110
Chloride (mg L ⁻¹)	310 ± 30	34 ± 6
λ _{max}	258 nm	270 nm

^a The effluent was twice filtered through whatman paper (No. 42)

electrolyte containing precursor salts and subjected to ultrasonication for 5 min to replace the trapped air in the TiO₂-NTs with electrolyte solution. The impregnation of TiO₂-NTs with the electrolyte favors the initial growth of Sb-SnO₂. A primary layer of Sb-SnO₂ was loaded into TiO₂-NTs by square wave pulsed electrodeposition at an average current density of -2.5 mA cm^{-2} for 1800 s. After that, a secondary layer was deposited in a fresh electrolyte under similar conditions at an average current density of -5 mA cm^{-2} for 900 s. Finally, the electrode was annealed at 520 °C for 60 min under heating and cooling rate of 5 °C min^{-1} .

Electrode characterization

Scanning electron microscope (SEM, Tecan Vega-3 LMU, made in Czech Republic) equipped with energy-disperse spectrometer analyzer (EDS) (Ametek, USA) was used to examine the surface morphology and composition of the fabricated electrodes. The crystallographic features of TiO₂-NTs substrate and electrodeposited Sb-SnO₂ were characterized by grazing angle (1°) X-ray diffraction analysis using Cu K α radiation ($\lambda = 1.5406 \text{ \AA}$) in the 2θ range from 10 to 80° (scan rate 4° min^{-1} , Rigaku, Smartlab XRD, 40 kV, 30 mA). The crystallite size of SnO₂ determined by Scherrer equation (Eq. 1) was found to be 14.5 nm.

$$D = \frac{0.89 \lambda}{\beta \cos\theta} \quad (1)$$

where ' λ ' is 1.5418 Å (X-ray wavelength Cu-K α), ' β ' is full width at half maximum intensity (radians), ' θ ' is Bragg diffraction angle.

Diffuse reflectance UV-Visible spectra (UV-DRS) were recorded using UV-Vis spectrophotometer (HR 4000, UV-Vis-NIR light source, DT-MINI-2-GS, Jaz detector). BaSO₄ standard was used as reference material for UV-DRS analysis.

Accelerated service life test

The stability of TiO₂-NTs/Sb-SnO₂ electrode was estimated by accelerated service life test in 1 M H₂SO₄ by chronopotentiometry at an anodic current density of 200 mA cm^{-2} . The time taken for the electrode potential to increase by 5 V from the initial value was taken as the accelerated service life of the electrode and the electrode was considered as deactivated at this stage. The real-time service life of the electrode operated at different current densities and different electrolytes can be estimated by the relation (Eq. 2) as described by Hine et al. (1979).

$$\frac{t_1}{t_2} = \frac{(j_2)^n}{(j_1)^n} \quad (2)$$

where t_1 and t_2 are the service lifetime of the electrode, tested at the current densities j_1 and j_2 , respectively. ' n ' lies between 1.2 and 2 and depends on the wastewater matrix. Here, $n = 1.7$ was used for calculation.

Electrochemical experiments

The electrochemical experiments were carried out using CH instrument 660 C-electrochemical work station (USA) in a conventional three electrode system. The Ag/AgCl/KCl (3 M) was used as reference electrode in all experiments unless otherwise mentioned. A platinum wire was used as auxiliary electrode and the experiments were carried out at room temperature. Surface area of 1 cm^2 of the working electrode was exposed during the experiments. The cyclic voltammetry (CV) experiments were carried out to evaluate the active surface of the electrode. CV at different scan rates in the selected potential ranges was recorded in 0.25 M Na₂SO₄ solution.

To determine the presence of electroactive species in the effluents, TiO₂-NTs/Sb-SnO₂ electrode was allowed to attain constant OCP in 0.25 M Na₂SO₄ solution prepared in ultra-pure water (blank) and effluents. Once constant OCP was attained, the CV was recorded in the potential range of 0.3 to 3.0 V at a scan rate of 50 mV s^{-1} . The linear sweep voltammetry was recorded in the potential range 0.3–3.0 V at a scan rate of 50 mV s^{-1} .

Electrochemical impedance spectroscopy (EIS) was recorded in the AC frequency range from 100,000 to 0.1 Hz with 5 mV amplitude at different initial electrode potential from 1.5 V to 2.0 V. The results thus obtained were fitted using ZSimpWin software. The electrochemical equivalent circuit for which measurement error in the impedance data was less than 3% was considered as the best fit.

The photoelectrocatalytic activity of TiO₂-NTs/Sb-SnO₂ electrode was evaluated by transient photocurrent measurement at 1.5 V in 0.25 M Na₂SO₄ solution with or without ethylene glycol (EG) (0.5% v/v) in a quartz beaker of 100-mL volume capacity. A high-pressure mercury vapor lamp (HPMVL, $\lambda_{\text{max}} = 365 \text{ nm}$, 125 W Philips, India) was used as UV light source, and the photo-power density on the electrode surface was adjusted to 10 mW cm^{-2} using HTC-LX-101A Lux-meter.

Electrochemical and photo-assisted electrochemical degradation and analysis

A volume of 50 mL of industrial effluent was taken in a quartz beaker of 100-mL capacity and electrolyzed under constant stirring using magnetic bar (550 rpm) to achieve proper mixing and reproducible mass transport onto the electrode surface. The electrolytic system was kept in a water bath with

continuous water circulation to maintain room temperature. A DC power source (model PS 618 potentiostat/galvanostat 302/2, Chem-link, Mumbai) was used for constant current supply. A platinum foil (0.5 cm²) was used as cathode, and it was sonicated in 10% HNO₃ for 10 min and thoroughly washed with Millipore water prior to the experiments. The as-prepared TiO₂-NTs/Sb-SnO₂ was used as anode. The photo-assisted electrochemical oxidation was carried out under similar conditions in presence of UV light irradiation, and power density of 10 mW cm⁻² was maintained by adjusting the distance between the UV light and the quartz beaker. The HPMVL was placed in a cylindrical quartz water jacket, and continuous water circulation was maintained during the electrolysis to avoid rise in temperature of the system. The UV-lamp radiated predominantly at 365 nm (3.4 eV) and photon flux of 5.8 × 10⁻⁶ mol of photons sec⁻¹. The light radiation was made only to fall directly on the anode surface as shown in Fig. 1.

The % COD removal was determined after continuous electrolysis of 50 mL of effluent for 1 h. A volume of 30 mL of the electrolyzed sample was taken for COD (mg (O₂) L⁻¹) analysis by dichromate open reflux method (American standard test method D1252-06), and the % COD removal was calculated using Eq. (3). The reduction in absorbance at λ_{max} = 258 nm for TWW and λ_{max} = 270 nm for CWW was determined using a UV-Vis spectrophotometer (Ocean-Optics, HR 4000, UV-Vis-NIR light source, DT-MINI-2-GS). A volume of 0.5 mL of the electrolyzed sample diluted with 0.5 mL of ultrapure water was used for recording absorbance. The % reduction in absorbance was calculated using Eq. (4). Newly prepared TiO₂-NTs/Sb-SnO₂ electrodes and fresh effluent samples (50 mL) were used for each subsequent electrolysis experiments for 2, 3, 4, and 5 h. The electrodes were first characterized, and then, the electrodes with identical and best

electrochemical characteristics were selected for the electrochemical and photo-electrochemical oxidation.

$$COD\ removal, \% = \frac{COD_0 - COD_t}{COD_0} \times 100 \tag{3}$$

where COD₀ and COD_t are the COD in mg L⁻¹ at time 0 and t, respectively.

$$Absorbance\ reduction, \% = \frac{Abs_0 - Abs_t}{Abs_0} \times 100 \tag{4}$$

where Abs₀ and Abs_t are the absorbance at time 0 and t, respectively.

The average current efficiency (ACE) was calculated using Eq. (5), and the total energy consumed during the EO and PEO experiments was calculated by Eq. (6).

$$ACE, \% = \frac{[\Delta COD] F V_l}{8 I t} \times 100 \tag{5}$$

$$E, kWh (kgCOD)^{-1} = \frac{I \cdot t \cdot V \cdot 1000}{V_l \Delta COD} \tag{6}$$

where E is the total energy consumed, F is the Faraday's constant (96,485 C mol⁻¹), ΔCOD (mg L⁻¹) is the change in COD from time = 0 to t, I is the current (A), V_l is the volume (L) of electrolyte, t is the time (s), 8 = gram equivalent mass of oxygen (g equiv.⁻¹), V is the average cell voltage.

Result and discussion

Electrode characterization

The scanning electron microscopy (SEM) images showed regular vertically oriented TiO₂-NTs array with average pore diameter of 70 to 80 nm and wall thickness of 15 to 25 nm (Fig. 2a). The nanotube array of TiO₂-NTs provided large surface area and high specific volume for metal oxide loading. The impregnation of electrolyte facilitated initial deposition of Sb-Sn alloy inside TiO₂-NTs. A two-step pulsed electrodeposition process was carried out to obtain gradient electrodeposition of Sb-SnO₂ metal oxide. A primary layer of Sb-SnO₂ was loaded into TiO₂-NTs at an average current density of -2.5 mA cm⁻² for 1800 s (Fig. 2b). On the surface of this primary layer, a secondary layer was deposited using a fresh electrolyte under similar conditions at an average current density of -5 mA cm⁻² for 900 s. The surface morphology of the resulted TiO₂-NTs/Sb-SnO₂ electrode is shown in Fig. 2c. The rate of nuclei growth exceeds the rate of nuclei formation at low current density, due to steady discharge of Sn ions. Thus, a coarsely crystalline deposit was obtained at low current density. The rate of nuclei formation exceeds the rate of nuclei growth and thus the deposit obtained at higher current density was fine-grained (Watanabe 2004; Sung 2011; Ashutosh

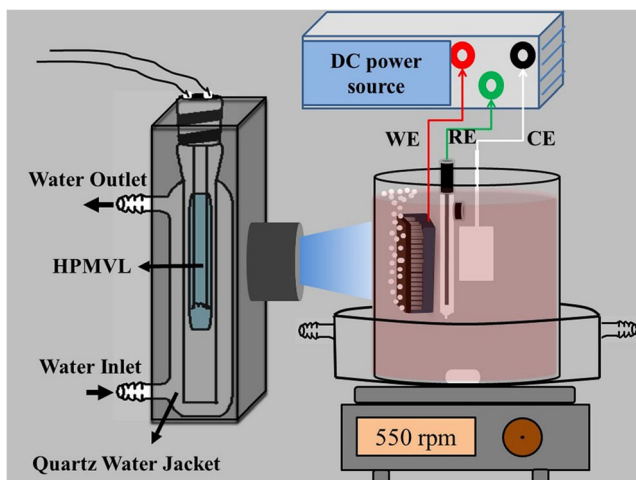
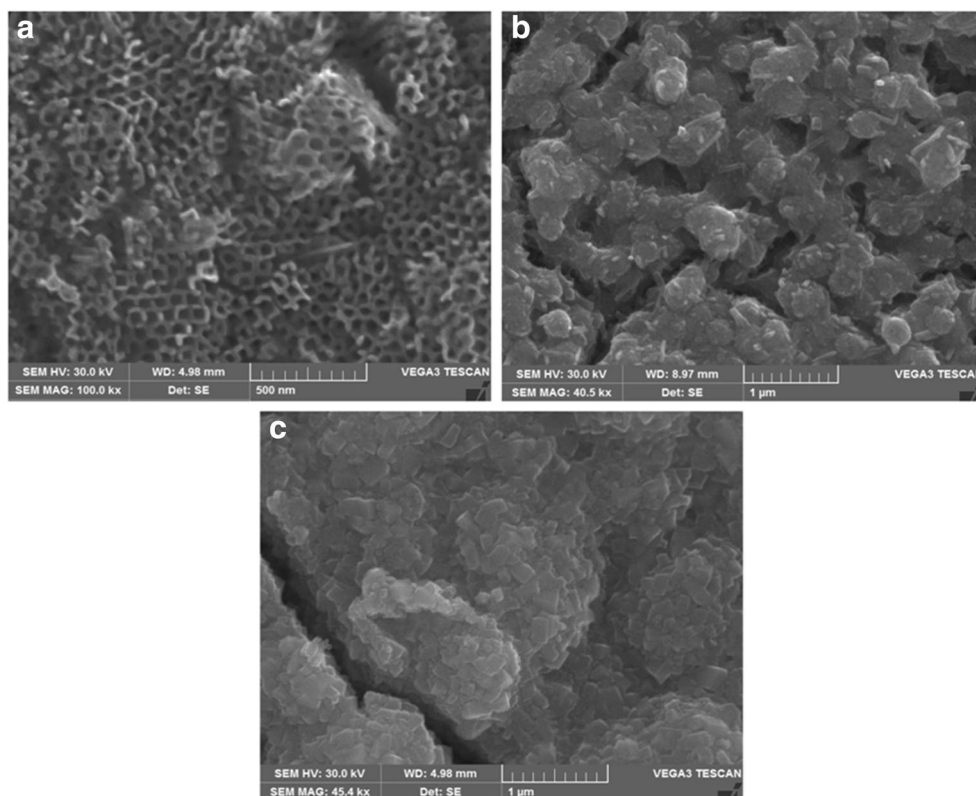


Fig. 1 Schematic diagram of photo-assisted electrochemical oxidation. WE–working electrode; RE–reference electrode; CE–counter electrode; HPMVL–high pressure mercury vapor lamp

Fig. 2 SEM images of **a** TiO₂-NTs, **b** primary layer of Sb-SnO₂ loaded into TiO₂-NTs by square wave pulsed electrodeposition at an average current density of -2.5 mA cm^{-2} for 1800 s, **c** Sb-SnO₂ loaded TiO₂-NTs by square wave pulsed electrodeposition at an average current density of -5 mA cm^{-2} for 900 s



et al. 2012). The overpotential increases with increase in current density and promotes the nucleation process. The Sb-SnO₂ deposition was more compact and the grain size significantly reduced on electrodeposition at higher current density.

The elemental composition of electrode surface was analyzed by energy dispersive spectroscopy (Fig. 3 and Table 2). The Sn and Sb present on the surface of mixed metal oxide coating correspond to a mixture of 70.8% SnO₂ and 29.2% Sb₂O₄. The absence of Ti peaks in the EDS of TiO₂-NTs/Sb-SnO₂ electrode indicated complete coverage of TiO₂-NTs substrate by metal oxide coating.

The diffraction peaks corresponding to TiO₂-anatase and TiO₂-rutile phase can be observed in Fig. 4a, and these peaks were absent in the XRD of TiO₂-NTs/Sb-SnO₂ electrode (Fig. 4b). This result further confirms the complete coverage of TiO₂-NT substrate by Sb-SnO₂ layer. The XRD patterns of Sb-SnO₂ electrode matched with the tetragonal SnO₂ (JCPDS 41-1445). The major three peaks of SnO₂ correspond to (110), (101), and (211) planes. The peaks corresponding (111), (112), and (004) planes of orthorhombic Sb₂O₄ (JCPDS 78-2066) were also observed. The electrode surface was thus a solid solution of SnO₂ and Sb₂O₄ metal oxides. The crystallite size of SnO₂ determined by Scherrer equation was found to be 14.5 nm.

Electrochemical characteristics of the electrode

The EIS of TiO₂-NTs/Sb-SnO₂ electrode was obtained in 0.25 M Na₂SO₄ solution at room temperature, and the

experimental data was fitted with the electrochemical equivalent circuit (EEC). The capacitance element was replaced with a constant phase element (CPE), whose contribution to the impedance is given by Eq. (7) (Punith Kumar et al. 2009);

$$Z(j\omega) = (Q)^{-1} (j\omega)^{-n} \quad (7)$$

where Z is the impedance, Q is the CPE constant, j is the imaginary unit, ω is the angular frequency, and 'n' is the measure of capacitance dispersion; $1 \geq n \geq -1$. Figure 5a is the Nyquist plot obtained on TiO₂-NTs/Sb-SnO₂ electrode and the best EEC fit is also shown as inset.

The Nyquist plot of TiO₂-NTs/Sb-SnO₂ electrode presented two electrochemical processes (Oury et al. 2012). The EEC consisted of three CPEs (Q_1 , Q_2 , and Q_3) and four resistance components (R_e , R_1 , R_2 , and R_{ct}). The calculated EIS data are tabulated in Table 3.

The component R_e in the high-frequency region is the electrolyte resistance due to concentration polarization. The Nyquist plot presents one resistance in the higher frequency region, two capacitive resistive semicircles in the middle frequency region, and one more capacitive resistance located in the low-frequency region. The capacitive loop in the low frequency region reduced in size with increase in applied potential as shown in Bode plots (Fig. 5c). According to the brick model, in a polycrystalline material, the grain boundary separates the stereo-network of crystal grains (Tigang et al. 2015).

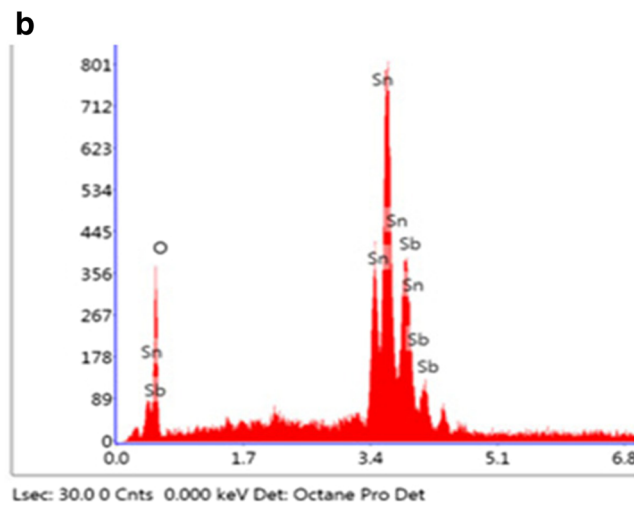
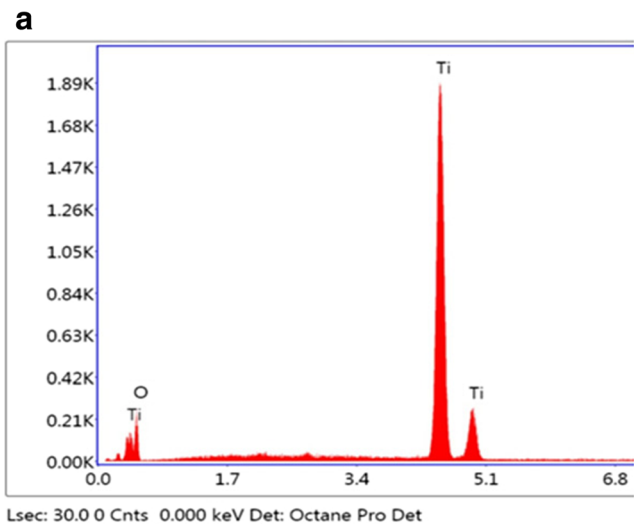


Fig. 3 EDS of **a** TiO₂-NTs, **b** TiO₂-NTs/Sb-SnO₂

The grains and grain boundaries are associated with different resistivity. The middle frequency region semicircles can be assigned to the grains and the low frequency semicircle can be assigned to the grain boundaries (Tigang et al. 2015). The electrochemical reaction in the present case can be attributed to the growth of resistive hydrated layer and adsorption-desorption of the intermediates generated during the oxygen evolution reaction which corresponds to two capacitances (Q₁ and Q₂) and corresponding resistances R₁ and R₂ (Punith Kumar et al. 2009; Tigang et al. 2015). The charge transfer process at the electrode–electrolyte interface is in series with the capacitive resistance. The charge transfer resistance (R_{ct}) is

Table 2 Chemical composition of the electrode surface

Electrode	EDS value (atomic %)			
	Sn	Sb	Ti	O
TiO ₂ -NTs	–	–	65.40	34.60
TiO ₂ -NTs/Sb-SnO ₂	30.04	12.39	–	57.56

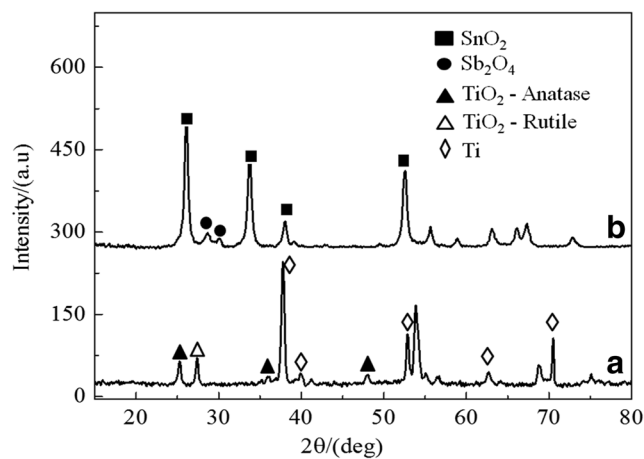


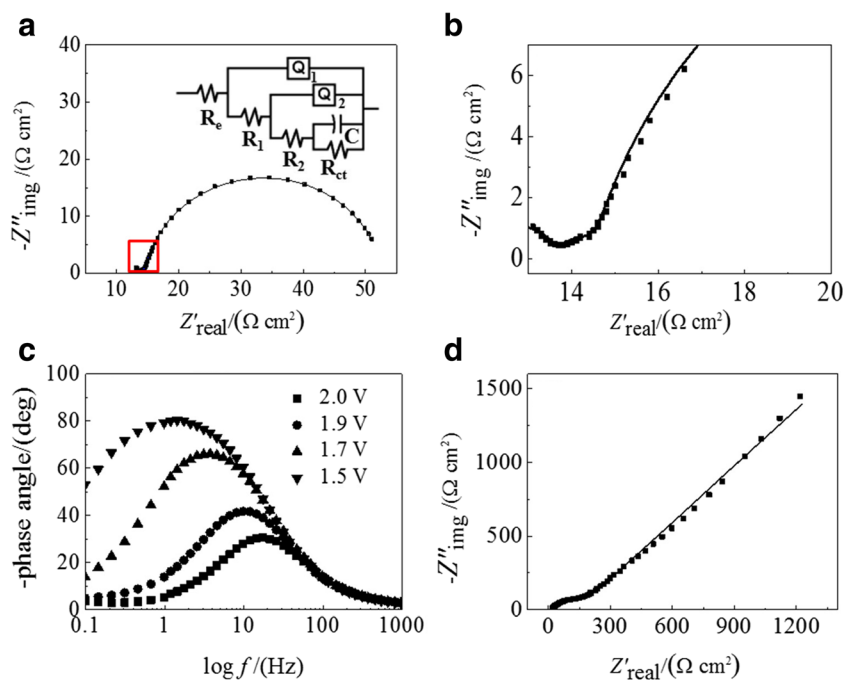
Fig. 4 X-ray diffractogram of **a** TiO₂-NTs, **b** TiO₂-NTs/Sb-SnO₂

a measure of the electrocatalytic activity of the electrode. The low-frequency semicircle in the Nyquist plot is related to a constant phase element (Q₃), and in the present case, the electrode surface acted as pure capacitor. The performance of the electrode is largely dependent on Q₃ and R_{ct}. The discharge process on the electrode surface is governed by the adsorption/desorption resistance of the species forming the hydrated layer rather than R_{ct}. The electrocatalytic activity of TiO₂-NTs/Sb-SnO₂ electrode is dependent on R₁-R₂ and Q₁-Q₂ as well. The impedance of TiO₂-NTs substrate significantly reduced from 175 kΩ to 52 Ω on Sb-SnO₂ loading. This can be attributed to the dispersion of conductive metal oxide inside the TiO₂ nanotubes (Peiqiang et al. 2009).

The charge buildup on the non-active electrode surface-solution interface is the non-Faradaic capacitance. The magnitude of this capacitance can be determined by the CV obtained in the narrow potential ranges where the electrochemical reactions are deprived (Berenguer et al. 2009). The CV scans were performed between 0.5 and 0.6 V, and the capacitance at the center of this potential range (0.55 V) was obtained by the absolute slope of current density vs scan rate plot as given in Fig. 6. The linear increase in current density with scan rate indicated non-Faradaic character (Berenguer et al. 2009). The obtained capacitance was compared with that of a smooth SnO₂-based electrode (C*) whose capacitance was taken to be 8 μF cm⁻² (Berenguer et al. 2009). The roughness factor (R_f) was obtained by the ratio C/C* which gives the real surface area of the electrode. The roughness factor at 0.55 V was found to be 154.41. The high R_f indicated the existence of large number of active sites on the electrode surface which facilitate the mass transfer of organics on to the electrode surface and lead to higher organic removal rate (Berenguer et al. 2009). The charge buildup reduced with increase in potential and charge transfer reaction dominated. The R_f calculated at different potentials is given in Table 4.

The accelerated service life test was carried out in 1 M H₂SO₄ under vigorous stirring at a constant anodic current

Fig. 5 Electrochemical impedance spectrum obtained in 0.25 M Na₂SO₄. Nyquist plots using **a** TiO₂-NTs/Sb-SnO₂; experimental data (symbols) and fitted data (solid line); **b** magnified portion of highlighted portion in **a**; **c** Bode plots at different initial input potentials; **d** Nyquist plot on TiO₂-NTs



density of 200 mA cm⁻² at room temperature (Fig. 6c). The service life of TiO₂-NTs/Sb-SnO₂ electrode was found to be ~ 31 h, which is comparable with the reported results (Martinez-Huitile and Ferro 2006; Guohua et al. 2009; Peiqiang et al. 2009; Xiao et al. 2009; Yong et al. 2010; Hao et al. 2012; Martinez-Huitile et al. 2015; Weiyi et al. 2015). The real-time service life of TiO₂-NTs/Sb-SnO₂ electrode working at a current density of 15 mA cm⁻² was estimated to be 2544 h.

The CV and LSV were conducted in 0.25 M Na₂SO₄ and effluents containing 0.25 M Na₂SO₄. The peaks corresponding to direct electron exchange reaction with the organics were absent. Therefore, the active oxidants generated on the electrode surface by electrolysis were responsible for the oxidative degradation of organics. The OEP on the TiO₂-NTs/Sb-SnO₂ electrode surface was 2.2 V (Fig. 6d) comparable with that observed by Ciriaco et al. (2001).

The UV-Visible DRS and Kubelka Munk plots of TiO₂-NTs substrate and TiO₂-NTs/Sb-SnO₂ electrode are given in Fig. 7a, b, respectively. The UV-DRS of TiO₂-NTs substrate showed high absorption below 400 nm wavelength. On loading Sb-SnO₂ metal oxide into the TiO₂-NTs substrate, UV-DRS spectrum showed significant reduction in the absorption intensity. The Kubelka-Munk plot was used to determine the absorbance and the band gap. The band gap of TiO₂-NTs was

found to be 2.8 eV, whereas for TiO₂-NTs/Sb-SnO₂ electrode, it was 3.2 eV. In this work, TiO₂-NTs substrate was used only as a structural support to bind the Sb-SnO₂ metal oxide onto the Ti substrate and to increase the loading capacity.

The transient photocurrent density measurement using TiO₂-NTs and TiO₂-NTs/Sb-SnO₂ electrodes is given in Fig. 7c, d). The increase in current density in presence of UV-light is due to the formation of electron-hole pair and involvement of these carriers in the electrochemical reactions (Nishanthi et al. 2015). The transient photocurrent density on TiO₂-NTs/Sb-SnO₂ electrode was much lower than that of TiO₂-NTs. This suggested significant reduction in photocatalytic activity of the electrode on Sb-SnO₂ loading. The photocurrent density measured in 0.25 M Na₂SO₄ using TiO₂-NTs/Sb-SnO₂ was found to be 30 μA cm⁻², and it increased to 55 μA cm⁻² in presence of radical scavenger-ethylene glycol. The photocurrent density measured in TWW and CWW was not much different from that obtained in 0.25 M Na₂SO₄.

Electrochemical and photoelectrochemical treatment of wastewater

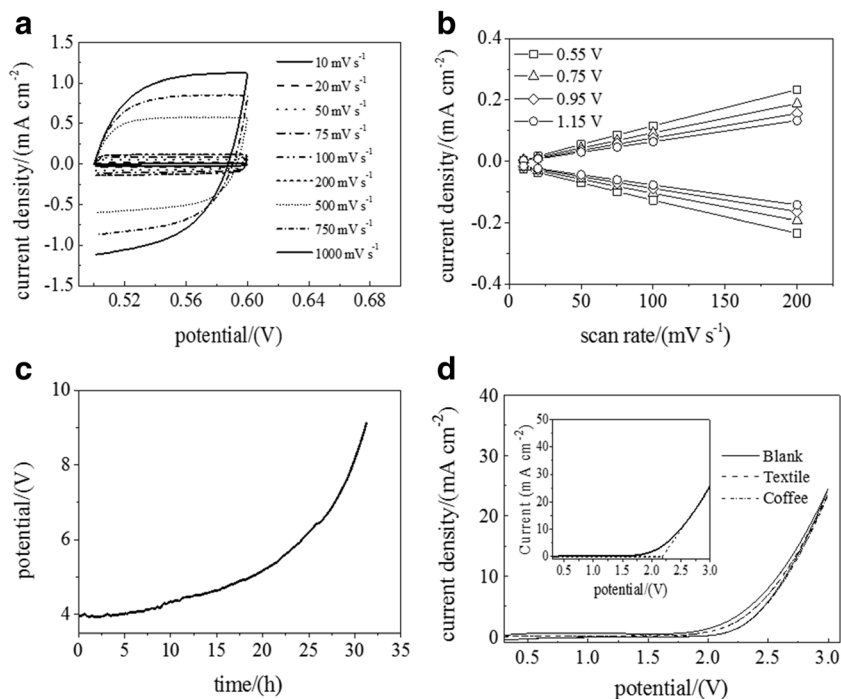
The chloride ion concentration was adjusted to 1000 ± 50 mg L⁻¹ in the wastewater samples. The electrolysis was

Table 3 EIS results as determined by the EEC fit

Electrode	*R _e	*R ₁	#CPE ₁	n ₁	*R ₂	#CPE ₂	n ₂	*R _{ct}	#CPE ₃	n ₃
TiO ₂ -NTs/Sb-SnO ₂	11.49	1.29	63.79	1.00	37.91	0.642	0.90	2.16	51.40	0.93

*Units in Ω cm² and # units in mF cm⁻²

Fig. 6 **a** CV at different scan rates in 0.25 M Na₂SO₄, **b** current density vs scan rate plot, **c** accelerated service life tested in 1 M H₂SO₄; current density—200 mA cm⁻² **d** CV in 0.25 M Na₂SO₄ in presence and absence of effluents; inset—LSV at a scan rate of 50 mV s⁻¹



carried out at room temperature without making any further chemical changes to the wastewater samples. The addition of NaCl not only increased the conductivity but also provided Cl⁻ ions for the generation of active chlorine species like HOCl, ⁻OCl, and Cl₂ on electrolysis. These oxidants, along with the hydroxyl radical, mediated the oxidative degradation of organics in TWW and CWW.

Prior to actual treatment process, preliminary tests were performed to examine the effect of current density on % COD and color removal using 50-mL wastewater sample. The results showed that the % COD removal at the end of 3 h increased linearly with increase in current density (Fig. 8a). This can be attributed to the increase in concentration of in situ generated oxidants at the anode surface with increase in applied current density. The operating current density was so chosen that at least ~40% reduction in COD was achieved from the initial value at the end of 5-h electrolysis. EO and PEO experiments were carried out under the applied current density of 30 mA cm⁻² for TWW and 50 mA cm⁻² for CWW, respectively. The reduction in COD and absorbance was not

observed either in TWW or CWW only on exposure to UV light for 5 h.

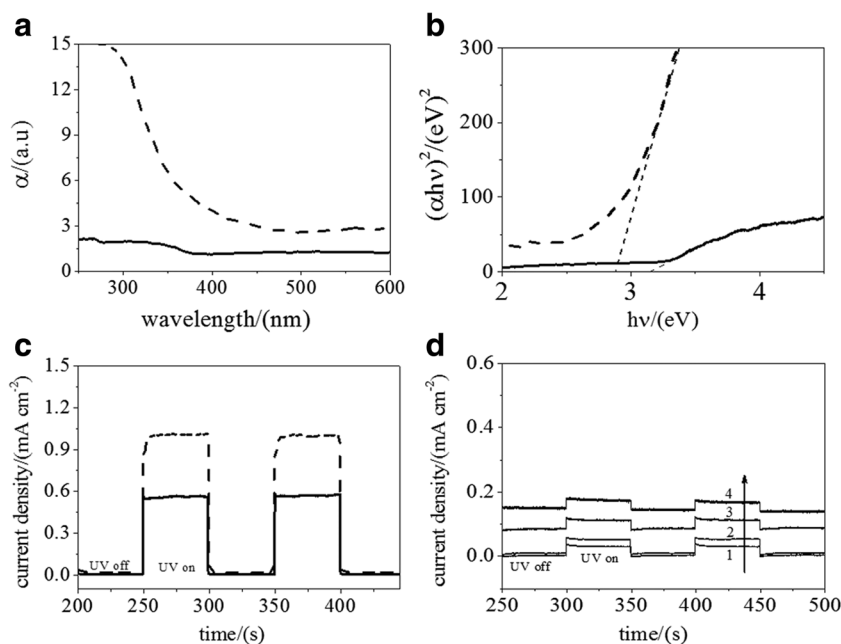
The degradation of organics was monitored by COD analysis. The % COD removal determined at regular intervals of time is given in Fig. 8b. The COD removal achieved at the end of 5 h of EO was only ~41% in both cases. However, under PEO, considerable enhancement in the COD removal was observed. The COD removal at the end of 5 h for TWW was 58%, and for CWW, it was 54%. More than 14% increment in the COD removal was observed under UV illumination.

The changes observed in the UV-Visible spectrum of two wastewater samples under EO and PEO conditions are as shown in Fig. 9. The UV-Visible spectrum of TWW showed one peak of maximum absorption intensity (λ_{max}) at 257 nm (Figs. 9a and 10). The components of TWW are unknown; however, the λ_{max} indicates that the core chromophore of the organic component is α , β -unsaturated carbonyl group. On electrolysis, the intensity of this peak reduced sharply and shifted to 264 nm. The bathochromic shift and disappearance of this peak can be ascribed to the oxidation reactions and subsequent degradation of the parent molecule. However, a new peak at 233 nm emerged and persisted even after 5 h. This peak can be attributed to the low molecular weight oxidized fragments like simple carboxylic acid residues, aromatic ring, and triazine rings in which $n \rightarrow \pi^*$ and $\pi \rightarrow \pi^*$ transitions are allowed ($-C=O$, $-C=C-$, $-C=N-$, $-(CO)NH-$), which are formed during the oxidative degradation (Luo et al. 2012; Anantha and Venkatesha 2013). The % reduction in the absorbance at the end of EO was only 55% (Fig. 8c). Under UV

Table 4 The capacitance at different potentials obtained by the anodic current density vs scan rate plot and R_f at 0.55 V of MMO-WO₃ and MMO electrodes determined in 0.25 M Na₂SO₄

Potential/V	Capacitance in mF cm ⁻²
0.55	1.23
0.75	1.00
0.95	0.82
1.05	0.70
R _f (0.55)	154.41

Fig. 7 **a** UV-DRS spectrum; **b** Kubelka Munk plot; **c** transient photocurrent measurement at 1.5 V (vs Ag/AgCl) using TiO₂-NTs in 0.25 M Na₂SO₄ (solid line) and in 0.25 M Na₂SO₄ + 0.5% v/v ethylene glycol (dashed line); **d** transient photocurrent measurement using TiO₂-NTs/Sb-SnO₂ in 0.25 M Na₂SO₄ (line 1); in 0.25 M Na₂SO₄ + 0.5% v/v ethylene glycol (line 2); in CWW with 0.25 M Na₂SO₄ (line 3); in TWW with 0.25 M Na₂SO₄ (line 4)



irradiation, the intensity of the peak at 257 nm reduced rapidly and remarkable enhancement in the reduction of peak intensity by 18% as compared to that observed by EO (Fig. 9b). At the end of 5 h, 73% reduction in the absorption peak intensity was observed under PEO.

In case of CWW, two major peaks were observed at wavelength 270 and 237 nm. These peaks could be assigned to the α , β -unsaturated carbonyl compounds, anthracene, and aromatic compounds in CWW. On electrolysis, the peak intensity

at 270 nm reduced slowly with time, and at the end of 5 h, it diminished completely. However, the peak at 237 nm reduced in intensity but remained intact even after the electrolysis for 5 h. The % reduction in the absorbance at λ_{max} was only 61%. Under PEO, both peaks at 270 and 237 nm reduced drastically. The peak at 270 nm disappeared completely and the intensity of the peak at 237 nm reduced significantly. The % reduction in the absorbance at the end of 5 h under PEO was observed to be 85%. The increment in the reduction of

Fig. 8 **a** Effect of current density on % COD removal, **b** % COD removal with time under EO and PEO conditions, **c** % reduction in UV-Visible absorbance at wavelength of maximum absorption with time, **d** variation of $\ln(C_0/C_t)$ with time

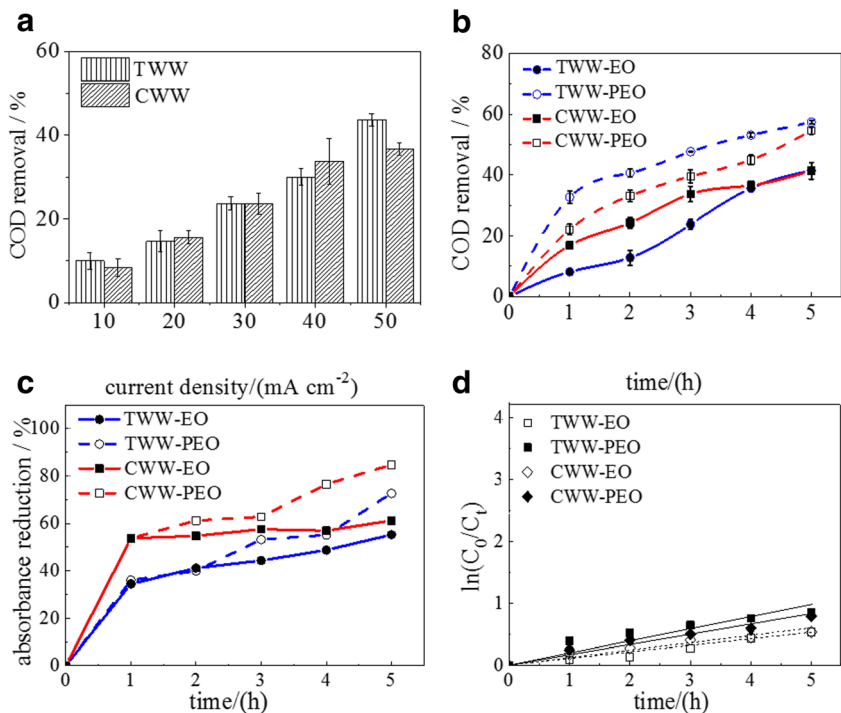
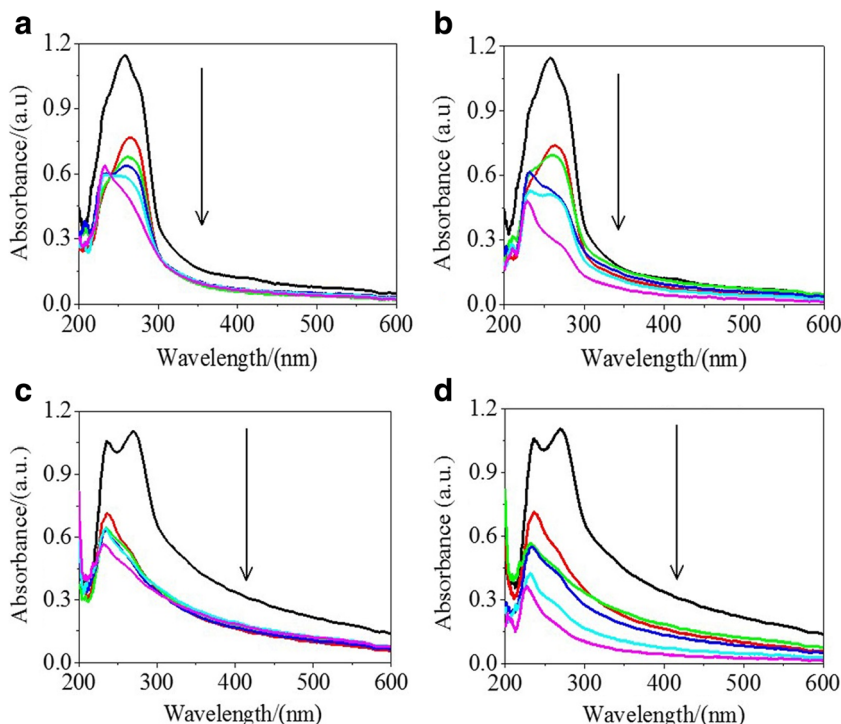


Fig. 9 Variation in the UV-Visible spectrum of TWW under **a** EO, **b** PEO and CWW under **c** EO and **d** PEO was determined at regular time intervals of 1 h during electrolysis. The color of the line corresponds to electrolysis time; black 1 h; red 2 h; green 3 h; blue 4 h; cyan 5 h; magenta 6 h



absorbance was 24%, which is significantly higher than that observed under EO. The reason is due to the photochemical oxidation of organics that take place on UV-irradiation on the O₂ gas evolved during electrolysis in PEO, which is not feasible by EO.

The COD decreased exponentially with time and the plot of Ln(C₀/C_t) vs time is a straight line, which indicates that the COD removal by EO or PEO followed pseudo first-order kinetics according to Eq. (8) (Fig. 8d).

$$\ln \frac{COD_0}{COD_t} = k_{app} \cdot t \tag{8}$$

where *k_{app}* is the apparent rate constant.

The apparent rate constant (*k_{app}*) for the COD removal in case of TWW by EO and PEO using TiO₂-NTs/Sb-SnO₂

electrode was found to be 1.7 × 10⁻³ and 3.2 × 10⁻³ min⁻¹, respectively. The rate of removal of COD under PEO was ~ 1.9 times as high as it was under EO, whereas for CWW, the *k_{app}* was found to be 2.0 × 10⁻³ and 2.7 × 10⁻³ min⁻¹ under EO and PEO, respectively. The *k_{app}* increased by 1.3 times from EO to PEO for CWW.

The turbidities of the wastewater samples were analyzed before and after EO and PEO (Fig. 11). These results showed that the initial turbidity of TWW reduced from 15 to ~ 3 NTU and in case of CWW turbidity reduced from 27 to ~ 3 NTU by both EO and PEO after 5 h. The turbidity in wastewater is mainly due to the presence of colloidal particles made up of organic compounds. These organic pollutants responsible for the turbidity in water were successfully removed and the colored turbid wastewater samples became clear and colorless after 5 h by both EO and PEO.

The energy consumption in kWh/kg (COD) was calculated to be 292.4 and 211.2 under EO and PEO, respectively for TWW, whereas for CWW, the energy required for the removal 1 kg COD was 411.0 and 311.2 kWh under EO and PEO, respectively. The estimated energy consumption corresponds to the COD removal observed at the end of 5 h electrolysis. These data are in accordance with the efficiency in COD removal as presented above.

The electrochemically generated hydroxyl radicals are responsible for the degradation of organics by EO (Yong et al. 2010). The enhancement in the rate of % COD removal under PEO can be attributed to two factors: (a) the photocatalytic activity of Sb-SnO₂ and (b) the secondary oxidants generated by the photolysis of electrogenerated O₂ and H₂O₂. The

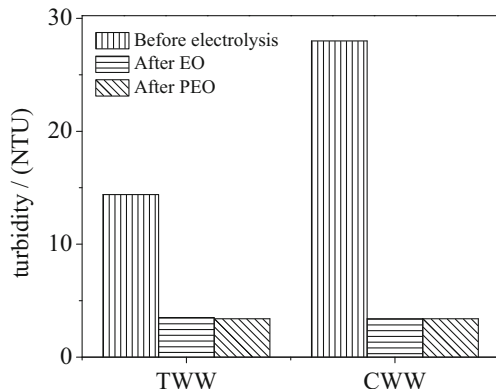


Fig. 10 Turbidity of TWW and CWW before and after electrolysis for 5 h by EO and PEO

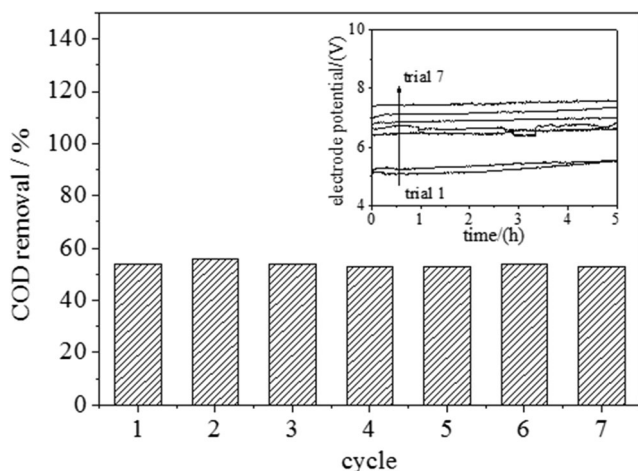
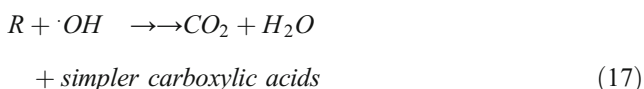
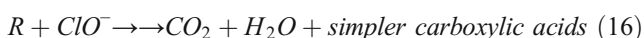
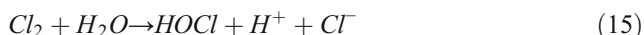
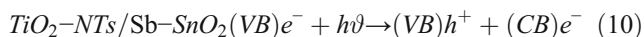
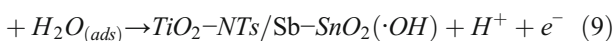


Fig. 11 COD removal (%) on using the same electrode for 7 cycles. Inset shows the variation in electrode potential with each cycle

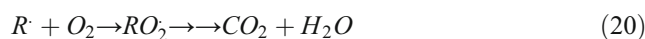
photocatalytic activity of Sb-SnO₂ in the present case was illustrated by the transient photocurrent measurement. The electron/hole pairs generated on irradiation of TiO₂-NTs/Sb-SnO₂ with UV migrate to the surface and participate in the redox reactions at the catalyst–electrolyte interface (Hao et al. 2011). In presence of external positive bias, the separation of charge carriers can be achieved. The photogenerated electrons are driven towards the cathode via the electrical circuit and the hole migrates to the surface of the electrode. The surface bound H₂O or ⁻OH is converted into hydroxyl radical on reaction with the photogenerated holes. The dissolved oxygen in water forms superoxide on reacting with the electrons at cathode. These reactive oxygen species participate in the oxidative degradation of organics (Anantha et al. 2017; Chin and Be 2005; Gupta et al. 2007; Md. Tamez et al. 2012; Nishanthi et al. 2015).

TiO₂-NTs/Sb-SnO₂



However, the photocatalytic activity of Sb-SnO₂ was found to be very small and cannot solely contribute to the increment in COD removal observed under PEO. Under the given

conditions (> 30 mA cm⁻²) of electrolysis, the oxygen evolution at the anode surface was the major secondary reaction other than hydroxyl radical formation. The photo-assisted electrochemical generation of reactive oxygen species (⁻OH or ⁻OOH), electrochemically generated active chlorine species, and peroxy radicals produced by O₂ on reaction organic radicals and subsequent photochemical reactions in presence of UV radiation are responsible for the significant enhancement in the COD removal under PEO (Egerton 1949; Emad and Raghad 2013; Anantha et al. 2017).



In order to examine the stability and reproducible performance of the fabricated electrode, the same electrode was repeatedly used to treat fresh CWW sample of 50 mL volume for 5 h by PEO. The performance of the electrode in each cycle is represented in Fig. 11. The % COD removal achieved at the end of each cycle remained constant and it was around 53 ± 3%. The % COD removal was consistent throughout the 7 cycles. However, the inset of Fig. 11 shows that the electrode potential required for maintaining constant current density (50 mA cm⁻²) gradually increased with each cycle. The electrode potential increased from 5.1 to 7.5 V vs saturated calomel electrode after 7 repeated PEO cycles. The increase in electrode potential is an indication of deactivation of electrode surface. Though the electrode surface was deactivated with each cycle, the consistent % COD removal was maintained by the reactive oxidants produced on electrolysis. The chloride media hampers the stability of the metal oxide electrode (Costa et al. 2010). Furthermore, the conductivity of the wastewater sample was less, and therefore, the potential required to maintain the current density was high. At such high potentials, the oxygen evolution reaction dominates and damages metal oxide coating. This results in passivation of the electrode as the electrolyte meet the substrate material.

Conclusions

The Ti/TiO₂-NTs/Sb-SnO₂ mixed metal oxide electrode was successfully fabricated by pulsed electrodeposition method. The as-prepared Ti/TiO₂-NTs/Sb-SnO₂ electrode exhibited high OER, stability, conductivity, and electrocatalytic activity for the decontamination of real industrial wastewaters. The high service life and reusability of the electrode were confirmed by the consistent performance of the electrode for 7 repeated cycles. The textile and coffee industrial wastewater was successfully treated by photoelectrochemical oxidation method under extremely mild conditions. The efficiency of

the electrochemical oxidation method enhanced remarkably on UV-irradiation.

Acknowledgments The authors thank the Department of Chemistry, Kuvempu University, Shankaraghatta for the laboratory facilities and University Grants Commission, New Delhi, India for financial support [F.No.41-231/2012(SR)]. The authors would like to thank Dr. Pavithra M. K, Lecturer, Department of chemistry, Kuvempu University, Shankaraghatta, India and Ms. Shilpi Samiksha, Research Scholar, Department of Earth and Environmental Science, Indian Institute of Science Education and Research, Bhopal, India for their suggestions in the execution of experiments and data interpretation.

References

- Anantha NS, Venkatesha TV (2013) Electrochemical treatment of trypan blue synthetic wastewater and its degradation pathway. *J Electrochem Sci Eng* 3(4):167–184
- Anantha NS, Venkatesha TV (2014) Metal oxide-coated anodes in wastewater treatment. *Environ Sci Pollut Res* 21:3197–3217
- Anantha NS, Venkatesha TV, Giridhar BN, Shubha HN, Pavithra MK (2017) Enhancement in the photo-electrocatalytic activity of SnO₂-Sb₂O₄ mixed metal oxide anode by nano-WO₃ modification: application to trypan blue dye degradation. *J Environ Chem Eng* 5:4969–4979
- Anlin X, Xiang D, Kajia W, Weiqing H, Jiansheng L, Xiuyun S, Jinyou S, Lianjun W (2017) Preparation and characterization of a TiO₂-NT/SnO₂-Sb tubular porous electrode with long service lifetime for wastewater treatment process. *RSC Adv* 7:37806–37814
- Ashutosh S, Sumit B, Ranjan S, Reddy BSB, Fecht HJ, Karabi D, Siddhartha D (2012) Influence of current density on microstructure of pulse electrodeposited tin coatings. *Mater Charact* 68:22–32
- Basha CA, Soloman PA, Velan M, Balasubramanian N, Roohil Kareem L (2009) Participation of electrochemical steps in treating tannery wastewater. *Ind Eng Chem Res* 48(22):9786–9796. <https://doi.org/10.1021/ie900046s>
- Berenguer R, Quijada C, Morallón E (2009) Electrochemical characterization of SnO₂ electrodes doped with Ru and Pt. *Electrochim Acta* 54(22):5230–5238. <https://doi.org/10.1016/j.electacta.2009.04.016>
- Carla RC, Francisco M, Emilia M, Paulo O (2010) Electrochemical oxidation of synthetic tannery wastewater in chloride-free aqueous media. *J Hazard Mater* 180:429–435
- Chatzisyseon E, Dimou A, Mantzavinos D, Katsaounis A (2009) Electrochemical oxidation of model compounds and olive mill wastewater over DSA® electrodes: 1. The case of Ti/IrO₂ anode. *J Hazard Mater* 167(1-3):268–274. <https://doi.org/10.1016/j.jhazmat.2008.12.117>
- Chin A, Be PR (2005) Removal of disinfection by-product precursors with ozone-UV advanced oxidation process. *Water Res* 39(10):2136–2144. <https://doi.org/10.1016/j.watres.2005.03.021>
- Ciriaco L, Santos D, Pacheco MJ, Lopes A (2001) Anodic oxidation of organic pollutants on a Ti/SnO₂-Sb₂O₄ anode. *J Appl Electrochem* 41:577–587
- Costa CR, Montilla F, Morallón E, Olivi P (2010) Electrochemical oxidation of synthetic tannery wastewater in chloride-free aqueous media. *J Hazard Mater* 180(1-3):429–435. <https://doi.org/10.1016/j.jhazmat.2010.04.048>
- Egerton GS (1949) The mechanism of the photochemical degradation of textile material. *J Soc Dyers Colours* 65:764–780
- Errami M, Saighi R, Zarrouk A, Zougagh M, Zarrok H, Hammouti B, Al-Deyab SS (2013) Electrochemical treatment of wastewater industrial cartons. *Int J Electrochem Sci* 8:12672–12682
- Emad Y, Raghad H (2013) Photodegradation and photostabilization of polymers, especially polystyrene: review. *SpringerPlus* 2(398):1–32
- Fan CM, Hua B, Wang Y, Liang ZH, Hao XG, Liu SB, Sun YP (2009) Preparation of Ti/SnO₂-Sb₂O₄ photoanode by electrodeposition and dip coating for PEC oxidations. *Desalination* 249(2):736–741. <https://doi.org/10.1016/j.desal.2009.01.035>
- Fengping H, Ziqiang D, Xinwei C, Weixing C (2011) Improved SnO₂-Sb₂O₄ based anode modified with Cr₃C₂ and CNT for phenol oxidation. *Electrochim Acta* 56:1576–1580
- Guohua Z, Xiao C, Meichuan L, Peiqiang L, Yonggang Z, Tongcheng C, Hongxu L, Yanzhu L, Lei L, Dongming L (2009) Electrochemical degradation of refractory pollutant using a novel microstructured TiO₂ nanotubes/Sb-doped SnO₂ electrode. *Environ Sci Technol* 43:1480–1486
- Gupta VK, Rajeev J, Alok M, Megha M, Shalini S (2007) Photochemical degradation of the hazardous dye safranin-T using TiO₂ catalyst. *J Colloid Interface Sci* 309(2):464–469. <https://doi.org/10.1016/j.jcis.2006.12.010>
- Hao A, Hao C, Wenyi Z, Jianping Z, Yan Q, Xianchun X, Qin L (2012) Fabrication and electrochemical treatment application of a microstructured TiO₂-NTs/Sb-SnO₂/PbO₂ anode in the degradation of C.I. Reactive blue 194 (RB 194). *Chem Eng J* 209:86–93
- Hao X, Qian Z, Wei Y, Chu W (2011) A composite Sb-doped SnO₂ electrode based on the TiO₂ nanotubes prepared by hydrothermal synthesis. *Int J Electrochem Sci* 6:6639–6652
- Hine F, Yasuda M, Noda T, Yoshida T, Okuda J (1979) Electrochemical behavior of the oxide-coated metal anodes. *Electrochem Sci Technol* 126(9):1439–1445
- Humberto RJ, Carlos BD, Ivonne LH, Cheikh F, Bilyeu B (2015) A combined electrocoagulation-electrooxidation process for carwash wastewater reclamation. *Int J Electrochem Sci* 10:6754–6767
- Jungeng N, Yang L, Enxiang S, Zesheng X, Jinzi L (2016) Electrochemical oxidation of perfluorinated compounds in water. *Chemosphere* 146:526–538
- Justin TJ, Oliver SS, Michael RH (2016) Electrochemical transformation of trace organic contaminants in latrine wastewater. *Environ Sci Technol* 50(18):10198–10208
- Luo J, Yang J, Li W, Huang Q, Xu H (2012) Electrochemical degradation of reactive brilliant red K-2BP on Ti/RuTiIrSnMn oxide anode in a batch cell. *J Electrochem Sci Eng* 2:171–183
- Martinez-Huitle CA, Ferro S (2006) Electrochemical oxidation of organic pollutants for the wastewater treatment: direct and indirect processes. *Chem Soc Rev* 35(12):1324–1340
- Martinez-Huitle CA, Rodrigo MA, Sires I, Scialdone O (2015) Single and coupled electrochemical processes and reactors for the abatement of organic water pollutants: a critical review. *Chem Rev* 115(24):13362–13407. <https://doi.org/10.1021/acs.chemrev.5b00361>
- Md. Tamez U, Yohann N, Celine O, Thierry T, Laurent S, Mathis M. M, Hans-Joachim K, Jurgen Z, Wolfram J. (2012). Nanostructured SnO₂-ZnO Heterojunction photocatalysts showing enhanced photocatalytic activity for the degradation of organic dyes. 51:7764–7773
- Nishanthi ST, Subramanian E, Sundarakannan B, Pathinettam Padiyan D (2015) An insight into the influence of morphology on the photoelectrochemical activity of TiO₂ nanotube arrays. *Solar Energy Mater Solar Cells* 132:204–209
- Oury A, Kirchev A, Bultel A (2012) Oxygen evolution on alpha-lead dioxide electrodes in methanesulfonic acid. *Electrochim Acta* 63:28–36. <https://doi.org/10.1016/j.electacta.2011.12.028>
- Panizza M, Cerisola G (2009) Direct and mediated anodic oxidation of organic pollutants. *Chem Rev* 109(12):6541–6569. <https://doi.org/10.1021/cr9001319>
- Patricia AC, Marly EO, Jeosadaque JS, Marc AA, Maria VBZ (2004) Evaluation of color removal and degradation of a reactive textile azo dye on nanoporous TiO₂ thin-film electrodes. *Electrochim Acta* 49:3807–3820

- Peiqiang L, Guohua Z, Xiao C, Yonggang Z, Yiting T (2009) Constructing stake structured TiO₂-NTs/Sb-doped SnO₂ electrode simultaneously with high electrocatalytic and photocatalytic performance for complete mineralization of refractory aromatic acid. *J Phys Chem C* 113:2375–2383
- Punith Kumar MK, Venkatesha TV, Pavithra MK, Nithyananda Shetty A (2009) The fabrication, characterization and electrochemical corrosion behavior of Zn-TiO₂ composite coatings. *Phys Scr* 84(3): 035601–035610
- Radjenovic J, Sedlak DL (2015) Challenges and opportunities for electrochemical processes as next-generation technologies for the treatment of contaminated water. *Environ Sci Technol* 49(19):11292–11302. <https://doi.org/10.1021/acs.est.5b02414>
- Rajkumar D, Palanivelu K (2004) Electrochemical treatment of industrial wastewater. *J Hazard Mater* 113(1–3):123–129. <https://doi.org/10.1016/j.jhazmat.2004.05.039>
- Sung HW (2011) Nanostructured metals and alloys, processing, microstructure, mechanical properties and applications. Woodhead publishing limited, Philadelphia
- Tigang D, Ye C, Qing W, Ying D (2015) Different mechanisms and electrocatalytic activities of Ce ion or CeO₂ modified Ti/Sb–SnO₂ electrodes fabricated by one-step pulse electrocodeposition. *RSC Adv* 5:19601–19612
- Wang B, Chang X, Ma H (2008) Electrochemical oxidation of refractory organics in the coking wastewater and chemical oxygen demand (COD) removal under extremely mild conditions. *Ind Eng Chem Res* 47(21):8478–8483. <https://doi.org/10.1021/ie800826v>
- Watanabe T (2004) Nano-plating microstructure control theory of plated film and database of plated film microstructure, 1st edn. Elsevier, Oxford
- Weiyi W, Zhao-Hong H, Teik-Thye L (2014) Recent development of mixed metaloxide anodes for electrochemical oxidation of organic pollutants in water. *Appl Catal B General* 480:58–78
- Weiyi W, Zhao-Hong H, Teik-Thye L (2015) Enhanced electrochemical oxidation of phenol using a hydrophobic TiO₂-NTs/SnO₂-Sb-PTFE electrode prepared by pulse electrodeposition. *RSC Adv* 5:32245–32255
- Xiao C, Guohua Z, Yanzhu L, Hongxu L, Peiqiang L, Meichuan L (2009) Novel vertically aligned TiO₂ nanotubes embedded with Sb-SnO₂ electrode with high oxygen evolution potential and long service life. *Mater Chem Phys* 113:314–321
- Yong C, Lei H, Hongmin X, Weiqing H, Lianjun W, Xiuyun S, Jiansheng L (2010) Preparation and characterization of TiO₂-NTs/SnO₂-Sb electrodes by electrodeposition. *J Electroanal Chem* 648:119–127
- Zhen L, Youting D, Weijun K, Cui L, Dong L, Xueyuan W, Zhiwen C, Minghong W, Dengyu P (2015) Reduction mechanism and capacitive properties of highly electrochemically reduced TiO₂ nanotube arrays. *Electrochim Acta* 161:40–47